Probing excitons and biexcitons in coupled quantum dots by coherent two-dimensional optical spectroscopy

E. G. Kavousanaki, O. Roslyak, and S. Mukamel
Department of Chemistry, University of California, Irvine, California 92617, USA
(Received 18 December 2008; published 29 April 2009)

We calculate two-dimensional (2D) photon-echo and double-quantum-coherence spectra of two coupled InGaAs/GaAs quantum dots at various distances, taking into account electron, hole, and exciton hopping. Signatures of direct and indirect excitons in two-exciton resonances are revealed. At short distances, electron delocalization contributes to the creation of new biexcitonic peaks, and dipole-dipole interactions shift the two-exciton energies.

DOI: 10.1103/PhysRevB.79.155324 PACS number(s): 78.47.Fg, 78.67.Hc

I. INTRODUCTION

The optical response of confined excitons in semiconductor quantum dots (QDs) has been studied extensively.[1–3] The ability to control their electronic properties makes them ideal candidates for studying fundamental many-body effects.[4–6] In addition, they are promising candidates for numerous applications, including fluorescence labels of biomolecules,[7] lasers,[8] solar cells,[9] and quantum computing.[10] Arrays of QDs were proposed as building blocks in quantum information applications, e.g., as a quantum register for noiseless information encoding.[11] Biexcitons have been suggested as a source of entangled photons.[12] Much effort has been devoted to the investigation of the coupling between the dots, either due to exciton[13,14] or carrier migration.[15–17] However, both coupling mechanisms may coexist, and separating them is of considerable interest.

Two-dimensional (2D) spectroscopy provides a new tool for studying coupled excitons in molecular aggregates,[18] photosynthetic complexes,[19] semiconductor quantum wells,[20] and QDs.[17,21] In these experiments, the system is subjected to three temporally well separated femtosecond pulses propagating in the directions $\mathbf{k}_1$, $\mathbf{k}_2$, and $\mathbf{k}_3$ and centered at times τ_1, τ_2, and τ_3 (Fig. 1). 2D signals of two coupled quantum wells were simulated recently using a free-carrier model, neglecting Coulomb interactions and many-body effects such as biexcitons.[22] In this paper, we shall calculate these signals for a system of two coupled quantum dots. This QD molecule is described by a tight-binding two-band Hamiltonian for electrons and holes,[23] taking into account interdot electron and hole hoping along with monopole-monopole and dipole-dipole Coulomb interactions. We use realistic parameters for the system studied in Refs. 16 and 24. The Hamiltonian is recast in terms of *e-h* pair variables, truncated at the two-exciton manifold.[25] We consider two types of heterodyne detected signals,[26] S_{I} and S_{III}, generated in the phase-matching directions $\mathbf{k}_{\mathrm{I}}=-\mathbf{k}_1+\mathbf{k}_2+\mathbf{k}_3$ (photon echo), and $\mathbf{k}_{\mathrm{III}}=+\mathbf{k}_1+\mathbf{k}_2-\mathbf{k}_3$ (double-quantum coherence), respectively. Both are recorded as a function of time delays $t_1=\tau_2-\tau_1$, $t_2=\tau_3-\tau_2$, and $t_3=t-\tau_3$, where t is the detection time. 2D spectra, obtained by a Fourier transform of S_{I} with respect to t_1 and t_3, $S_{\mathrm{I}}(\Omega_3,t_2,\Omega_1)$, and of S_{III} with respect to t_2 and t_3, $S_{\mathrm{III}}(\Omega_3,\Omega_2,t_1)$, reveal exciton correlations and two-exciton resonances.[27] The signals are obtained by solving the nonlinear exciton equations (NEE),[27,28] which account for exciton-exciton interactions and their quasibosonic nature.[17,29] To classify biexciton states in terms of their single-exciton constituents, we analyze both the S_{I} and S_{III} signals using the corresponding sum-over-states expressions (SOS).[27] The roles of different coupling mechanisms at various interdot distances d is discussed. We show that at short distances electron delocalization contributes to the creation of new biexcitonic peaks in the spectra, while exciton hopping shifts the two-exciton peaks.

In Sec. II we present our model Hamiltonian for two coupled quantum dots. In Sec. III we discuss the variation in the absorption spectra and single-exciton eigenstates with interdot distance. In Sec. IV we present the photon echo and double-quantum coherence spectra and identify the biexcitonic contributions. Summary and conclusions are given in Sec. V.

II. MODEL HAMILTONIAN FOR TWO COUPLED QUANTUM DOTS

We consider a system of two vertically stacked, lens-shaped InGaAs/GaAs QDs of height 2 nm and radius 10 nm aligned along the z axis.[24] It is described by the tight-binding two-band Hamiltonian,[23,30]

$$H_{\mathrm{QD}}=H_0+H_C. \tag{1}$$

Here H_0 represents noninteracting electrons and holes, and H_C are the Coulomb interactions. Due to quantum confine-

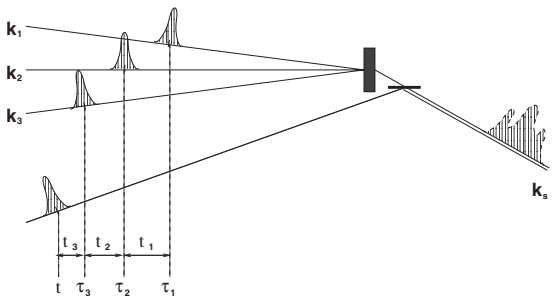

FIG. 1. The pulse sequence in a four-wave-mixing experiment: the system is excited by three pulses propagating at directions $\mathbf{k}_1$, $\mathbf{k}_2$, and $\mathbf{k}_3$ and centered at times τ_1, τ_2, and τ_3, respectively. The signal is heterodyne detected in the phase-matching direction $\mathbf{k}_s$ at time t.

ment, the conduction and valence bands split into discrete atomiclike levels. Each dot in InGaAs has two spin-degenerate electron states, with angular-momentum quantum numbers $(J,M)=(\frac{1}{2},\pm\frac{1}{2})$, and two heavy-hole states $(\frac{3}{2},\pm\frac{3}{2})$. The free-carrier Hamiltonian has the form,[17,28]

$$H_0=\sum_{m_1n_1} t^{(1)}_{m_1n_1}\hat{c}^\dagger_{m_1}\hat{c}_{n_1}+\sum_{m_2n_2} t^{(2)}_{m_2n_2}\hat{d}^\dagger_{m_2}\hat{d}_{n_2} \tag{2}$$

where the indices 1 (2) correspond to electrons (holes) in the conduction (valence) band. The subscripts, e.g., $m_1=(R_{m_1},\sigma_{m_1})$, describe the QD position $R=\{T,B\}$ ("T" for top and "B" for bottom) and the spin projection σ of the carrier ($\uparrow,\downarrow$ for up or down-spin projection, respectively). The creation and annihilation operators of an electron (hole) in site $R_{m_1}(R_{m_2})$ with spin z component $\sigma_{m_1}(\sigma_{m_2})$ are $\hat{c}^\dagger_{m_1}$ and $\hat{c}_{m_1}$ ($\hat{d}^\dagger_{m_2}$ and $\hat{d}_{m_2}$). These satisfy the Fermionic algebra,

$$\{\hat{c}_{m_1},\hat{c}^\dagger_{n_1}\}\equiv\hat{c}_{m_1}\hat{c}^\dagger_{n_1}+\hat{c}^\dagger_{n_1}\hat{c}_{m_1}=\delta_{m_1n_1}, \tag{3}$$

$$\{\hat{d}_{m_2},\hat{d}^\dagger_{n_2}\}=\delta_{m_2n_2}. \tag{4}$$

All other anticommutators are zero. The diagonal elements of $t^{(1)}$ and $t^{(2)}$ give the electron and hole energies, while off-diagonal elements represent carrier hopping in the conduction and valence bands, respectively.

The Coulomb interaction is

$$H_C=\frac{1}{2}\sum_{m_1n_1} V^{ee}_{m_1n_1}\hat{c}^\dagger_{m_1}\hat{c}^\dagger_{n_1}\hat{c}_{n_1}\hat{c}_{m_1}+\frac{1}{2}\sum_{m_2n_2} V^{hh}_{m_2n_2}\hat{d}^\dagger_{m_2}\hat{d}^\dagger_{n_2}\hat{d}_{n_2}\hat{d}_{m_2}-\sum_{m_1n_2} V^{eh}_{m_1n_2}\hat{c}^\dagger_{m_1}\hat{d}^\dagger_{n_2}\hat{d}_{n_2}\hat{c}_{m_1}+\sum_{\substack{m_1m_2n_1n_2\\ R_{m_1}=R_{m_2}\neq R_{n_1}=R_{n_2}}} V^F_{m_1m_2,n_1n_2}\hat{c}^\dagger_{m_1}\hat{d}^\dagger_{m_2}\hat{d}_{n_2}\hat{c}_{n_1}. \tag{5}$$

The first three terms are monopole-monopole contributions of electron-electron, hole-hole, and electron-hole interactions, respectively. Pseudopotential calculations, including strain and realistic band structure, have been performed for this system.[16,24] The on-site energies, hopping parameters, and Coulomb interaction energies have been reported vs interdot distance. Electrons tunnel at short ($\lesssim$8 nm) distances creating delocalized bonding and antibonding one-particle states. The heavy holes however remain localized, even at short $d(\lesssim 8$ nm), but their energies are lowered with decreasing distance. This is due to the high interdot barrier for the heavy holes, which suppresses hole tunneling (the heavy-hole-electron effective-mass ratio is $m_{hh}/m_e\approx 0.4/0.06\approx 6$), as well as to the effect of strain and band structure. We will use the parameters from Ref. 24, as listed in Table I, and assume $V^{ee}=V^{hh}=-V^{eh}$.

The last term in Eq. (5) describes the electrostatic dipole-dipole interactions between the charge distributions in the QDs which induce exciton hopping,[13,14,31]

TABLE I. Hamiltonian parameters for a system of two vertically stacked quantum dots, labeled as T (top) and B (bottom), obtained from Ref. 24: electron and hole on-site energies (E^e, E^h), tunneling couplings (t^e, t^h), as well as e-h Coulomb interaction elements (V^{eh}) vs interdot distance.

Parameter (meV)	Distance dependence (d in nm)
E^e_{T}	$1450-436d^{-1}+3586d^{-2}-7382d^{-3}$
E^e_{B}	$1449-452d^{-1}+3580d^{-2}-6473d^{-3}$
E^h_{T}	$167+129d^{-1}-2281d^{-2}+6582d^{-3}$
E^h_{B}	$163+274d^{-1}-3780d^{-2}+9985d^{-3}$
t_e	$-255\exp(-d/2.15)$
t_h	$-4.25\exp(-d/3.64)$
V^{eh}_{BB}	$-29.0+7.98/d$
V^{eh}_{TT}	$-29.6+19.6/d$
V^{eh}_{BT}	$-99.1/\sqrt{d^2+3.72^2}$
V^{eh}_{TB}	$-98.5/\sqrt{d^2+4.21^2}$

$$V^F_{m_1m_2,n_1n_2}=\frac{1}{\epsilon r^3_{mn}}\left[\boldsymbol{\mu}_{m_1m_2}\cdot\boldsymbol{\mu}_{n_1n_2}-\frac{3(\boldsymbol{\mu}_{m_1m_2}\cdot\mathbf{r}_{mn})(\boldsymbol{\mu}_{n_1n_2}\cdot\mathbf{r}_{mn})}{r^2_{mn}}\right], \tag{6}$$

where ϵ is the dielectric constant, $\boldsymbol{\mu}_{m_1m_2}$ is the interband dipole moment at site $R_{m_1}=R_{m_2}\equiv R_m$, and $r_{mn}=|R_m-R_n|$ is the distance between sites m and n. Equation (6) has been shown to be adequate for direct-gap semiconductor quantum dots of radius 0.5–2 nm even when they are almost in contact.[13,32]

The interaction with the optical field in the rotating wave approximation is described by the Hamiltonian,

$$H_{\mathrm{int}}(t)=-[\mathbf{E}(t)\cdot\hat{\mathbf{V}}^\dagger+\mathrm{H.c.}], \tag{7}$$

where $\hat{\mathbf{V}}=\Sigma_{m_1m_2}\boldsymbol{\mu}_{m_1m_2}\hat{d}_{m_2}\hat{c}_{m_1}$ is the dipole moment annihilation operator, and $\mathbf{E}(t)$ is the negative frequency part of the optical field. The interband dipole moment $\boldsymbol{\mu}_{m_1m_2}$ at site $R_{m_1}=R_{m_2}$ is given by[17,33]

$$\boldsymbol{\mu}_{\uparrow\uparrow}=\frac{\mu}{\sqrt{2}}(\hat{x}+i\hat{y})\quad \boldsymbol{\mu}_{\downarrow\downarrow}=\frac{\mu}{\sqrt{2}}(\hat{x}-i\hat{y}), \tag{8}$$

where $\hat{x}$ and $\hat{y}$ are the polarization directions of the optical pulses. The measured dipole moments in InGaAs quantum dots are $\mu=25-35$ D.[34]

The total Hamiltonian for the QD molecule-light system is

$$H=H_{\mathrm{QD}}+H_{\mathrm{int}}(t). \tag{9}$$

Using the method proposed by Chernyak and Mukamel,[25] Hamiltonian (9) can be transformed into the excitonic representation by introducing the electron-hole pair operators,

$$\hat{B}^{\dagger}_{m_1m_2} = \hat{c}^{\dagger}_{m_1}\hat{d}^{\dagger}_{m_2}, \quad \hat{B}_{m_1m_2} = \hat{d}_{m_2}\hat{c}_{m_1}. \tag{10}$$

The main steps of this transformation are given in Appendix A. The transformed Hamiltonian will be used in Secs. III and IV to study the one and two-exciton properties.

III. SINGLE-EXCITON MANIFOLD AND THE ABSORPTION SPECTRUM

The absorption spectrum was calculated by a Fourier transform of the linear response obtained by Eq. (B7). It is given by[26]

$$A(\omega) \propto \mathrm{Im}\left[\sum_e \frac{|\mu_{eg}|^2}{\omega - E_e + i\gamma_{eg}}\right], \tag{11}$$

where e denotes single-exciton states with energy E_e and dephasing rate γ_{eg}. We set γ=0.05 meV, obtained from the measured linewidths in a similar system.[15] The single-exciton block of the Hamiltonian has four fourfold spin-degenerate eigenstates. Since spin does not affect the absorption, we will drop it here, but include it in the nonlinear response in Sec. IV, since two-exciton states may be formed by single excitons of different spins.

The single-exciton eigenstates $|\alpha\rangle$, $|\beta\rangle$, $|\gamma\rangle$, and $|\delta\rangle$ are expanded in the basis (Fig. 2),

$$|a\rangle = \hat{c}^{\dagger}_{\mathrm{B}}\hat{d}^{\dagger}_{\mathrm{B}}|g\rangle \quad |c\rangle = \hat{c}^{\dagger}_{\mathrm{B}}\hat{d}^{\dagger}_{\mathrm{T}}|g\rangle$$

$$|b\rangle = \hat{c}^{\dagger}_{\mathrm{T}}\hat{d}^{\dagger}_{\mathrm{T}}|g\rangle \quad |d\rangle = \hat{c}^{\dagger}_{\mathrm{T}}\hat{d}^{\dagger}_{\mathrm{B}}|g\rangle \tag{12}$$

where B (T) denotes the bottom (top) QD, and $|g\rangle$ is the ground state. $|a\rangle$ and $|b\rangle$ describe direct excitons, while $|c\rangle$ and $|d\rangle$ are indirect excitons.

The variation of the simulated absorption spectra with interdot distance d is shown in Fig. 3. At large distances (d =17 nm), the two QDs are uncoupled and indirect excitons are optically forbidden. Because of QD slight asymmetry (see Table I), there are two peaks corresponding to direct excitons $|\alpha\rangle$=$|a\rangle$ and $|\beta\rangle$=$|b\rangle$.

As the distance is decreased, the absorption peaks are blueshifted and their splitting is reduced. This is due to the decreasing hole energies, as well as to the electron tunneling, which leads to carrier delocalization. As shown in Fig. 2, exciton splitting is minimized at d=8.6 nm, where the single-exciton eigenstates are approximately given by

$$|\alpha\rangle \approx |a\rangle + |b\rangle \quad |\gamma\rangle \approx |c\rangle,$$

$$|\beta\rangle \approx |a\rangle - |b\rangle \quad |\delta\rangle \approx |d\rangle, \tag{13}$$

with energies $E_\alpha \approx E_\beta < E_\gamma < E_\delta$. The QD-localized excitons at large d now become strongly entangled bonding and antibonding excitons. At the same time, indirect excitons appear. These are blueshifted since their binding energy is smaller than for the direct excitons, due to the reduced Coulomb attraction.

At shorter distances, the two lower excitons anticross, while the contribution of the two upper ones in the absorption spectrum become stronger. The exciton eigenstates now form bonding and antibonding states,

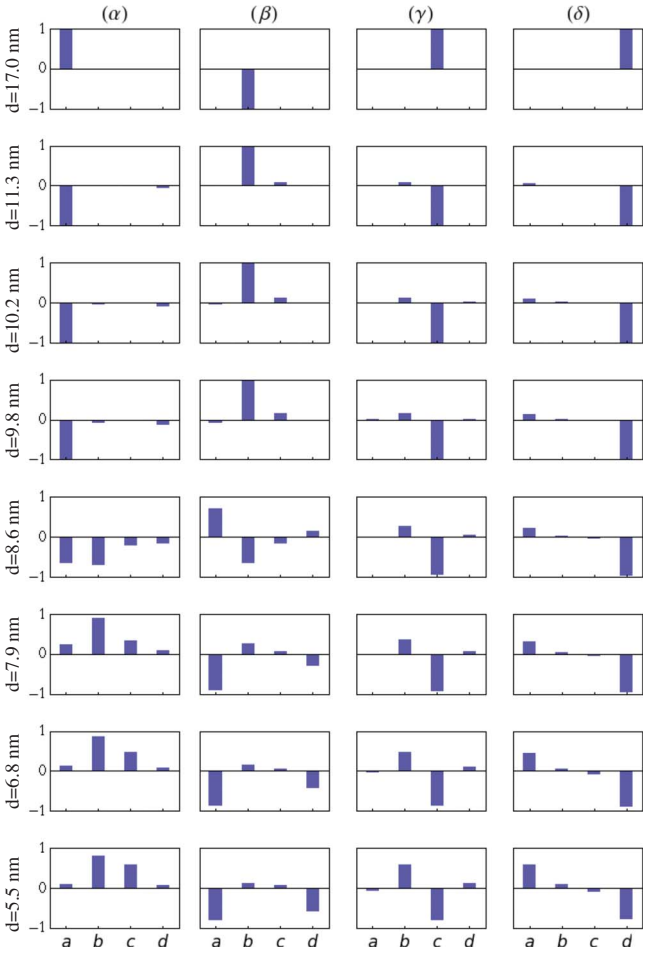

FIG. 2. (Color online) The four single-exciton eigenstates $|\alpha\rangle$, $|\beta\rangle$, $|\gamma\rangle$, $|\delta\rangle$ vs interdot distance, expanded in the e-h basis $|a\rangle$ (both particles in the bottom QD), $|b\rangle$ (both particles in the top QD), $|c\rangle$ (electron in the bottom and hole in the top QD), and $|d\rangle$ (electron in the top and hole in the bottom QD).

$$|\alpha\rangle \approx |b\rangle + |c\rangle \quad |\gamma\rangle \approx |b\rangle - |c\rangle,$$

$$|\beta\rangle \approx |a\rangle + |d\rangle \quad |\delta\rangle \approx |a\rangle - |d\rangle, \tag{14}$$

with energies $E_\alpha < E_\beta < E_\gamma < E_\delta$. Thus, the electron is delocalized but the hole is not. This is attributed to the smaller

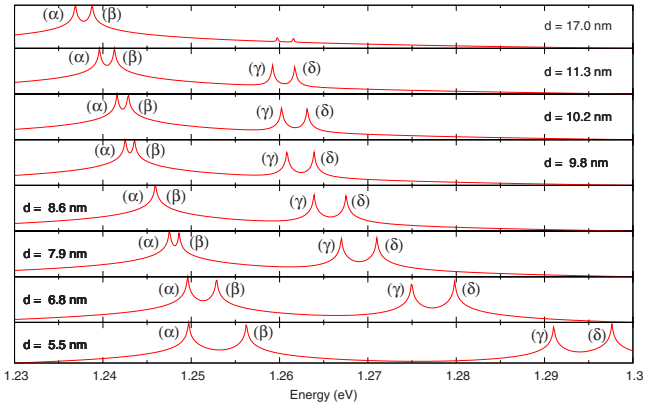

FIG. 3. (Color online) Absorption spectra (logarithmic scale) at various interdot distances d.

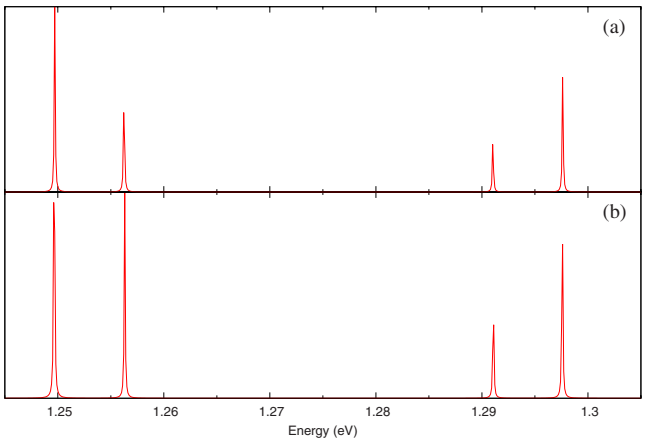

FIG. 4. (Color online) Absorption spectrum with (a) and with no (b) dipole-dipole interactions for the shortest interdot distance $d=5.5$ nm.

effective mass of the electron, as well as to the more complicated valence-band structure and the effect of strain, which favor hole localization.[24]

The effect of dipole-dipole interactions for the shortest distance, $d=5.5$ nm, is shown in Fig. 4. The peak positions are the same, but their intensity is changed. The more pronounced effect of dipole-dipole interactions in the nonlinear response will be discussed in Sec. IV.

IV. TWO-EXCITON MANIFOLD AND THE 2D SPECTRA

We focus on the two-exciton states and their energies E_f. The optical response is calculated using the NEE (Refs. 27 and 28) for the single- and two-particle variables $\langle \hat{B}_m \rangle$ and $\langle \hat{B}_m \hat{B}_n \rangle$ (Appendix B). The 2D spectra [Eqs. (C2) and (C9)] are calculated in terms of the single-exciton Green's functions and the exciton scattering matrix[27] (Appendix C).

All simulations were carried out using the SPECTRON package.[35] However, it is more convenient to analyze them using the alternative sum-over-states expressions[17]

$$S_{\mathrm{I}}^{\nu_4\nu_3\nu_2\nu_1}(\Omega_3, t_2=0, \Omega_1) = i \sum_{ee'} \frac{\mu_{ge'}^{\nu_1}}{\Omega_1 + E_{e'} + i\gamma_{e'g}} \times \left[\sum_f \frac{\mu_{eg}^{\nu_2} \mu_{fe}^{\nu_3} \mu_{e'f}^{\nu_4}}{\Omega_3 - E_f + E_{e'} + i\gamma_{fe'}} - \frac{(\mu_{eg}^{\nu_2} \mu_{e'g}^{\nu_3} + \mu_{e'g}^{\nu_2} \mu_{eg}^{\nu_3}) \mu_{ge}^{\nu_4}}{\Omega_3 - E_e + i\gamma_{eg}} \right], \tag{15}$$

$$S_{\mathrm{III}}^{\nu_4\nu_3\nu_2\nu_1}(\Omega_3, \Omega_2, t_1=0) = i \sum_{ee'f} \frac{\mu_{eg}^{\nu_1} \mu_{fe}^{\nu_2}}{\Omega_2 - E_f + i\gamma_{fg}} \times \left[\frac{\mu_{ge'}^{\nu_4} \mu_{e'f}^{\nu_3}}{\Omega_3 - E_f + E_{e'} + i\gamma_{fe'}} - \frac{\mu_{ge'}^{\nu_3} \mu_{e'f}^{\nu_4}}{\Omega_3 - E_{e'} + i\gamma_{e'g}} \right], \tag{16}$$

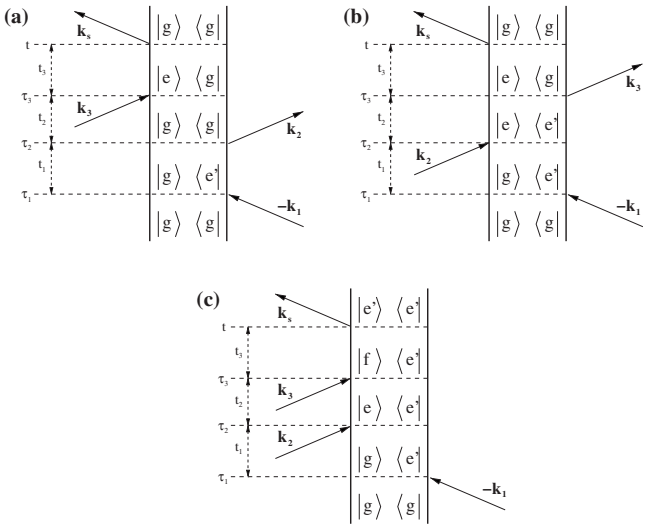

FIG. 5. Feynman diagrams for the $\mathbf{k}_{\mathrm{I}}$ technique.

where g denotes the ground state, e and e' are single excitons, and f is a doubly excited state. γ_{eg}, γ_{fe}, and γ_{fg} are the corresponding dephasing rates.

The $\mathbf{k}_{\mathrm{I}}$ signal shows resonances at single-exciton energies along the Ω_1 axis, at $\Omega_1=-E_{e'}$, and two types of resonances along Ω_3: at $\Omega_3=E_e$ and $\Omega_3=E_f-E_{e'}$. Thus, the diagonal peaks along $\Omega_3=-\Omega_1=E_e$ reveal single-exciton states, similar to the linear absorption, while the off-diagonal cross peaks reveal exciton coherences and biexciton contributions. To see which excitons contribute to the formation of each biexciton we turn to the Feynman diagrams, which represent the sequences of interactions with the optical fields and the state of the excitonic density matrix during the intervals between interactions.[35] For the $\mathbf{k}_{\mathrm{I}}$ technique, there are three diagrams, shown in Fig. 5: ground-state bleaching [(a)], stimulated emission [(b)], and excited-state absorption [(c)]. The two-exciton states f formed by excitons e and e' only show up in (c). Thus, a cross peak at ($\Omega_1=-E_{e'}$, $\Omega_3=E_f-E_{e'}$) indicates that exciton e' contributes to that biexciton.

The $\mathbf{k}_{\mathrm{III}}$ spectrum provides complementary information. As in $\mathbf{k}_{\mathrm{I}}$, the resonances along Ω_3 are at single-exciton energies $\Omega_3=E_{e'}$ and at $\Omega_3=E_f-E_{e'}$. Along Ω_2 though, the signal directly reveals two-exciton energies $\Omega_2=E_f$. There are two corresponding Feynman diagrams, shown in Fig. 6, which both describe excited-state absorption. The two-exciton state is formed by excitons e and e' and results in cross peaks at ($\Omega_2=E_f$, $\Omega_3=E_{e'}$) [(a)] or ($\Omega_2=E_f, \Omega_3=E_f-E_{e'}$) [(b)]. We thus obtain information on the contributing single-exciton states.

The variation in the $\mathbf{k}_{\mathrm{I}}$ signals with d is displayed in Fig. 7, and Fig. 8 shows the $\mathbf{k}_{\mathrm{III}}$ signals. At $d=17$ nm, direct excitons $|\alpha\rangle=|a\rangle$ and $|\beta\rangle=|b\rangle$ result in two diagonal peaks at E_α and E_β in the $\mathbf{k}_{\mathrm{I}}$ spectrum. Biexcitons can be formed either from excitons within the same QD, or from excitons in different QDs. Because of the slight asymmetry between the dots, there are two same-dot biexcitons (in the top or bottom QD), which create two closely spaced peaks, labeled A, in the $\mathbf{k}_{\mathrm{III}}$ spectrum [Fig. 8(a)] at $E_{f_1}=2360$ meV and $E_{f_2}=2363$ meV. In $\mathbf{k}_{\mathrm{I}}$ [Fig. 7(a)], they create two cross peaks at

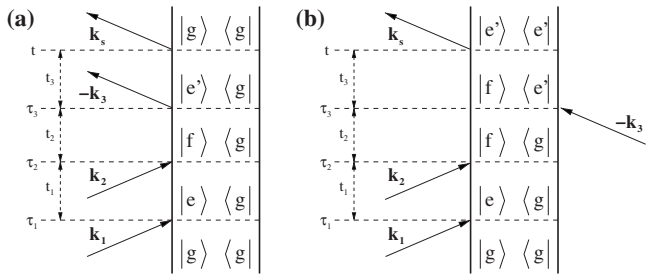

FIG. 6. Feynman diagrams for the $\mathbf{k}_{\mathrm{III}}$ technique.

$\Omega_3=E_{f_1}-E_\alpha$ and $E_{f_2}-E_\beta$. The absence of cross peaks at $\Omega_3=E_{f_1}-E_\beta$ and $E_{f_2}-E_\alpha$ implies that biexciton $f_1(f_2)$ is formed by two $|a\rangle$-type ($|b\rangle$-type) single excitons localized in the bottom (top) QD. The third biexciton, labeled B, has energy $E_{f_3}=2453$ meV, higher than the other two. As shown in the $\mathbf{k}_{\mathrm{I}}$ spectrum, it creates peaks at both $\Omega_3=E_{f_3}-E_\alpha$ and $E_{f_3}-E_\beta$, indicating that it is formed by one exciton on each QD ($|\alpha\rangle$ and $|\beta\rangle$).

At $d=10.2$ nm, the indirect excitons $|\gamma\rangle=|c\rangle$ and $|\delta\rangle=|d\rangle$ show up on the diagonal [Figs. 7(b), 7(c), 8(a), and 8(b)]. In the $\mathbf{k}_{\mathrm{III}}$ spectrum, there are three bound biexcitons, labeled A and B, while the remaining cross peaks are due to unbound two-exciton states at energies $2E_\alpha, E_\alpha+E_\beta, 2E_\beta$. The first two biexcitons (A) are formed from excitons within the same QD, as in $d=17$ nm case. The third biexciton (B) is formed mostly from exciton $|\beta\rangle=|b\rangle$ and a small contribution from $|\gamma\rangle=|c\rangle$, which is the first sign of electron delocalization.

The 2D spectra at the critical distance of $d=8.6$ nm, where the two lower excitons become degenerate, are shown in Figs. 7(c) and 8(c). The $\mathbf{k}_{\mathrm{III}}$ spectrum has four biexciton peaks at energies $E_{f_1}=2381$ meV and $E_{f_2}=2383$ meV (labeled A), $E_{f_3}=2457$ meV (B), and $E_{f_4}=2523$ meV (C). The remaining peaks, at energies $E_e+E_{e'}$ $(e,e'=\alpha,\ldots,\delta)$, are due to unbound two-exciton states. The $\mathbf{k}_{\mathrm{I}}$ spectrum shows that biexcitons A and B are mostly formed by the first two excitons, which are now delocalized and may not be attributed to a single QD. The excitons are represented by bonding and antibonding orbitals $|a\rangle\pm|b\rangle$. The last cross peak C consists mostly of the two higher single-exciton states, the indirect excitons $|c\rangle$ and $|d\rangle$.

At shorter distances ($d=6.8$ nm and $d=5.5$ nm), the electrons become delocalized and yield richer spectra, as shown in panels (d) and (e) of Figs. 7 and 8. Four sets of biexcitonic peaks now appear in $\mathbf{k}_{\mathrm{III}}$. At $d=5.5$ nm we observe eight biexcitonic peaks, at $E_{f_1}=2407$ meV, $E_{f_2}=2411$ meV (A), $E_{f_3}=2424$ meV, $E_{f_4}=2440$ meV, $E_{f_5}=2449$ meV (D), $E_{f_6}=2490$ meV (B), and $E_{f_7}=2560$ meV, $E_{f_8}=2574$ meV (C). Looking at region (I) of the $\mathbf{k}_{\mathrm{I}}$ spectrum [Fig. 7(b)] one can see that biexcitons f_1 and f_2 of group A and f_3 of group D are formed mostly from the bonding orbitals $|\alpha\rangle=|b\rangle+|c\rangle$ and $|\beta\rangle=|a\rangle+|d\rangle$. Similarly, regions (I) and (II) show that f_4 and f_5 of group D are formed mostly from the antibonding ones $|\gamma\rangle=|b\rangle-|c\rangle$ and $|\delta\rangle=|a\rangle-|d\rangle$. Region (II) also suggests that all single-exciton states contribute significantly to the formation of biexcitons B and C.

In Fig. 9 we display the $\mathbf{k}_{\mathrm{I}}$ spectra calculated by neglecting dipole-dipole interactions at short distances, $d=6.8$ and $d=5.5$ nm [compare with panels (d) and (e) of Fig. 7]. The lowest excitonic peak on the diagonal becomes stronger. Biexcitons A, formed by bonding orbitals, redshifts while the remaining biexcitonic peaks remain at the same position.

V. CONCLUSIONS

We have studied the single and double excitons in two coupled quantum dots and their variation with interdot distance. Our calculation takes into account both carrier tunneling and exciton migration via dipole-dipole interactions. The absorption spectra were used to classify the single-exciton states in terms of localized e-h pairs. The 2D spectra in directions $\mathbf{k}_{\mathrm{I}}=-\mathbf{k}_1+\mathbf{k}_2+\mathbf{k}_3$ and $\mathbf{k}_{\mathrm{III}}=+\mathbf{k}_1+\mathbf{k}_2-\mathbf{k}_3$ were calculated by means of NEE. Analysis of these spectra using the corresponding SOS expressions, allowed us to classify the biexcitons according to their single-exciton components. At large distances, only direct excitons are active, and two types of biexcitons are formed, either within or at different QDs. At shorter distances, we also see biexcitons created from indirect excitons. At distances where electron interdot tunneling becomes noticeable, additional biexcitonic peaks appear, providing a clear signature of electron delocalization. Exciton hopping is significant only at short distances, where it affects the intensity of the excitonic peaks and shifts the biexciton energies.

ACKNOWLEDGMENTS

This work was supported by the Chemical Sciences, Geosciences and Biosciences Division, Office of Basic Energy Sciences, Office of Science, U.S. Department of Energy and the National Science Foundation Grant No. CHE-0745892. We thank Darius Abramavicius and Steven Cundiff for many useful discussions. Figures of 2D spectra were produced using the program dat2eps-v3.2.pl written by Cyril Falvo.

APPENDIX A: RECAST OF THE ELECTRON-HOLE HAMILTONIAN USING EXCITONIC VARIABLES

By introducing the electron-hole pair operators [Eq. (10)] Chernyak and Mukamel recasted Hamiltonian (9), as well as the commutation relations of these operators, in terms of an infinite series of normally ordered operators $\hat{B}^\dagger$ and $\hat{B}$.[25,28,29] Since the Hamiltonian conserves the number of particles, each term contains an equal number of creation ($\hat{B}^\dagger$) and annihilation ($\hat{B}$) operators. For computing the third-order response, the Hamiltonian can be truncated at fourth order,

$$H=\sum_{mn}h_{mn}\hat{B}_m^\dagger\hat{B}_n+\sum_{mnkl}U_{mn,kl}\hat{B}_m^\dagger\hat{B}_n^\dagger\hat{B}_k\hat{B}_l - \sum_m[\boldsymbol{\mu}_m^*\cdot\mathbf{E}(t)\hat{B}_m^\dagger+\mathrm{H.c.}] \tag{A1}$$

where electron-hole pairs are denoted with Latin indices without subscript $m=(m_1,m_2)$, $n=(n_1,n_2)$, etc. The parameters h_{mn} and $U_{mn,kl}$ of the effective Hamiltonian can be determined by comparing successively order by order the matrix elements of Hamiltonians (9) and (A1) in the space of

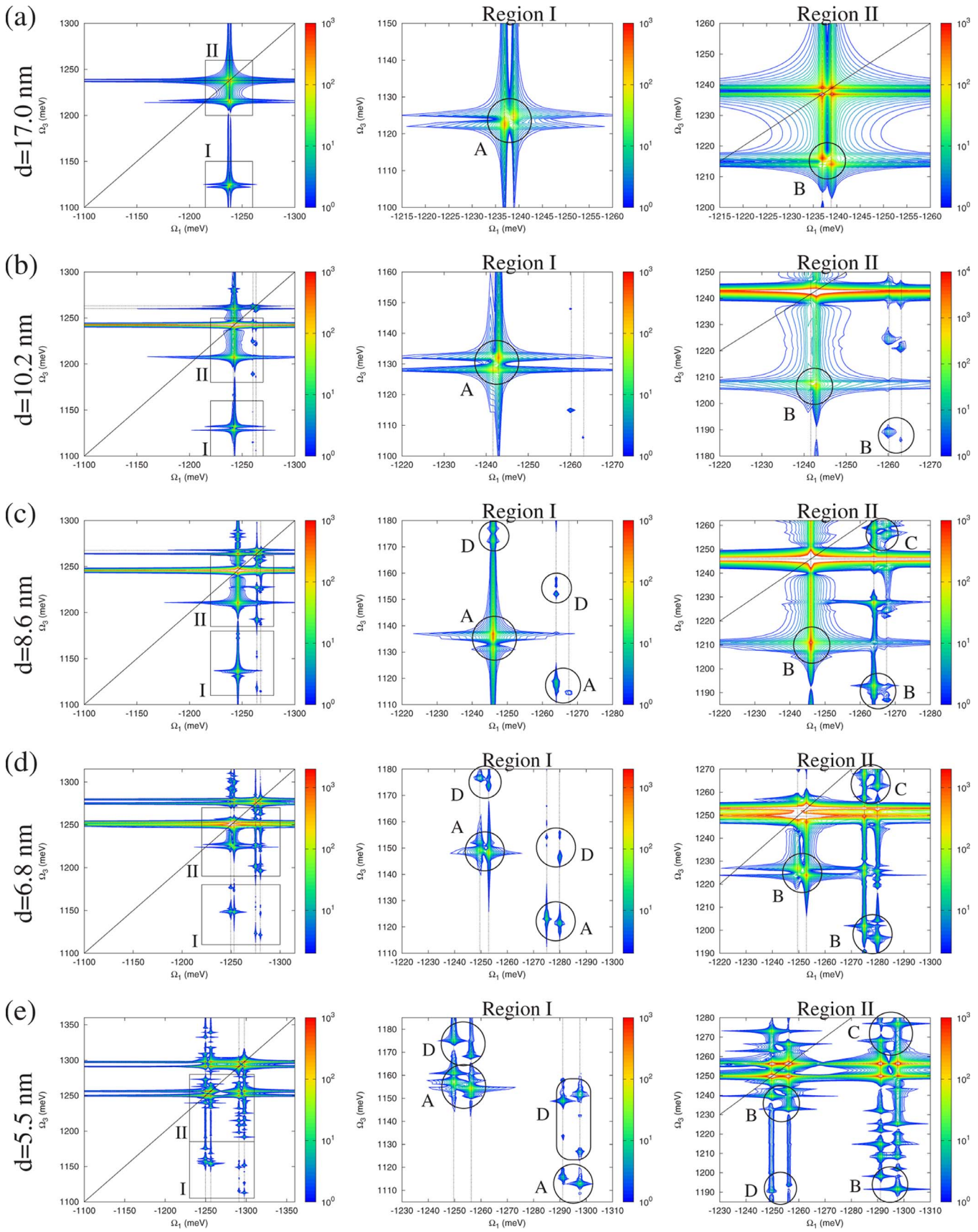

FIG. 7. (Color online) Absolute value of the $\mathbf{k}_I$ signal for *xxxx* polarization at several interdot distances *d*. Regions denoted as I and II are magnified in the center and right columns, respectively. Single-exciton energies are marked with dashed lines and biexciton peaks are circled.

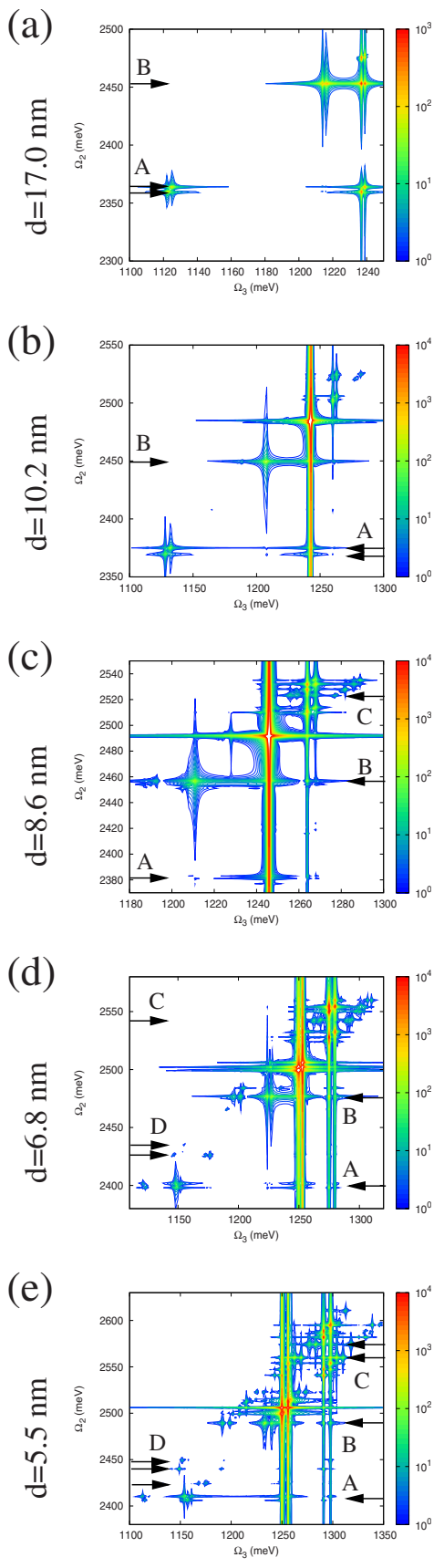

FIG. 8. (Color online) Absolute value of the $\mathbf{k}_{\mathrm{III}}$ signal for *xxxx* polarization at various interdot distances d. Arrows mark biexciton contributions.

one, two, three, etc. electron-hole pair excitations. This is possible because normally ordered N creation and N annihilation operators do not contribute in the subspaces of $N-1$ and smaller number of excitations. Thus, in the one electron-hole pair excitation subspace we obtain

$$h_{mn} = t^{(1)}_{m_1 n_1}\delta_{m_2 n_2} + \delta_{m_1 n_1} t^{(2)}_{m_2 n_2} - V^{eh}_{m_1 m_2}\delta_{m_1 n_1}\delta_{m_2 n_2} + V^{F}_{m_1 m_2, n_1 n_2}\delta_{R_{m_1} R_{m_2}}\delta_{R_{n_1} R_{n_2}}(1 - \delta_{R_{m_1} R_{n_1}}). \quad \text{(A2)}$$

Diagonal elements ($m=n$) describe the electron-hole pair energy, given as the sum of electron and hole kinetic energies reduced by the electron-hole Coulomb attraction. Off-diagonal elements ($m \neq n$) describe electron, hole, or exciton hopping between adjacent sites.

Similarly, to describe the one and the two electron-hole pair subspace we need the quartic term,

$$U_{mn,kl} = \bar{U}_{mn,kl} + F_{mn,kl}, \quad \text{(A3)}$$

where

$$\bar{U}_{mn,kl} = \frac{1}{4}[V^{ee}_{m_1 n_1}\delta_{m_1 l_1}\delta_{n_1 k_1}\delta_{m_2 k_2}\delta_{n_2 l_2} + V^{hh}_{m_2 n_2}\delta_{m_1 k_1}\delta_{n_1 l_1}\delta_{m_2 l_2}\delta_{n_2 k_2}] - \frac{1}{4}[t^{(1)}_{m_1 k_1}\delta_{m_2 k_2}\delta_{n_1 l_1}\delta_{n_2 l_2} + \delta_{m_1 k_1} t^{(2)}_{m_2 k_2}\delta_{n_1 l_1}\delta_{n_2 l_2} + \delta_{m_1 k_1}\delta_{m_2 k_2} t^{(1)}_{n_1 l_1}\delta_{n_2 l_2} + \delta_{m_1 k_1}\delta_{m_2 k_2}\delta_{n_1 l_1} t^{(2)}_{n_2 l_2}]. \quad \text{(A4)}$$

We further define the matrix F by the equation,

$$F_{mn,kl} + F_{mn,lk} - 2\sum_{pq} P_{mn,pq}F_{pq,kl} = 0. \quad \text{(A5)}$$

P is tetradic matrix defined as

$$P_{mn,pq} = \frac{1}{2}\delta_{m_1 q_1}\delta_{m_2 p_2}\delta_{n_1 p_1}\delta_{n_2 q_2} + \frac{1}{2}\delta_{m_1 p_1}\delta_{m_2 q_2}\delta_{n_1 q_1}\delta_{n_2 p_2}. \quad \text{(A6)}$$

The U matrix is invariant to the addition of any matrix F that satisfies Eq. (A5) and it is thus not uniquely defined. This freedom arises since Hamiltonians (9) and (A1) are only required to coincide in our physically relevant subspace of one and two e-h pair excitations but may differ in higher manifolds.

Similarly, the commutation relation of the electron-hole particle operators can be expanded in a series of normally ordered operators $\hat{B}^{\dagger}$ and $\hat{B}$. For the third-order response, this can be truncated at quadratic order,

$$[\hat{B}_m, \hat{B}^{\dagger}_n] = \delta_{mn} - 2\sum_{pq} P_{mp,nq}\hat{B}^{\dagger}_p \hat{B}_q, \quad \text{(A7)}$$

where $\delta_{mn} = \delta_{m_1 n_1}\delta_{m_2 n_2}$. The P matrix is responsible for the deviation from boson statistics.

APPENDIX B: THE NONLINEAR EXCITON EQUATIONS

The nonlinear optical response is calculated using the Heisenberg equation of motion for the electron-hole operator

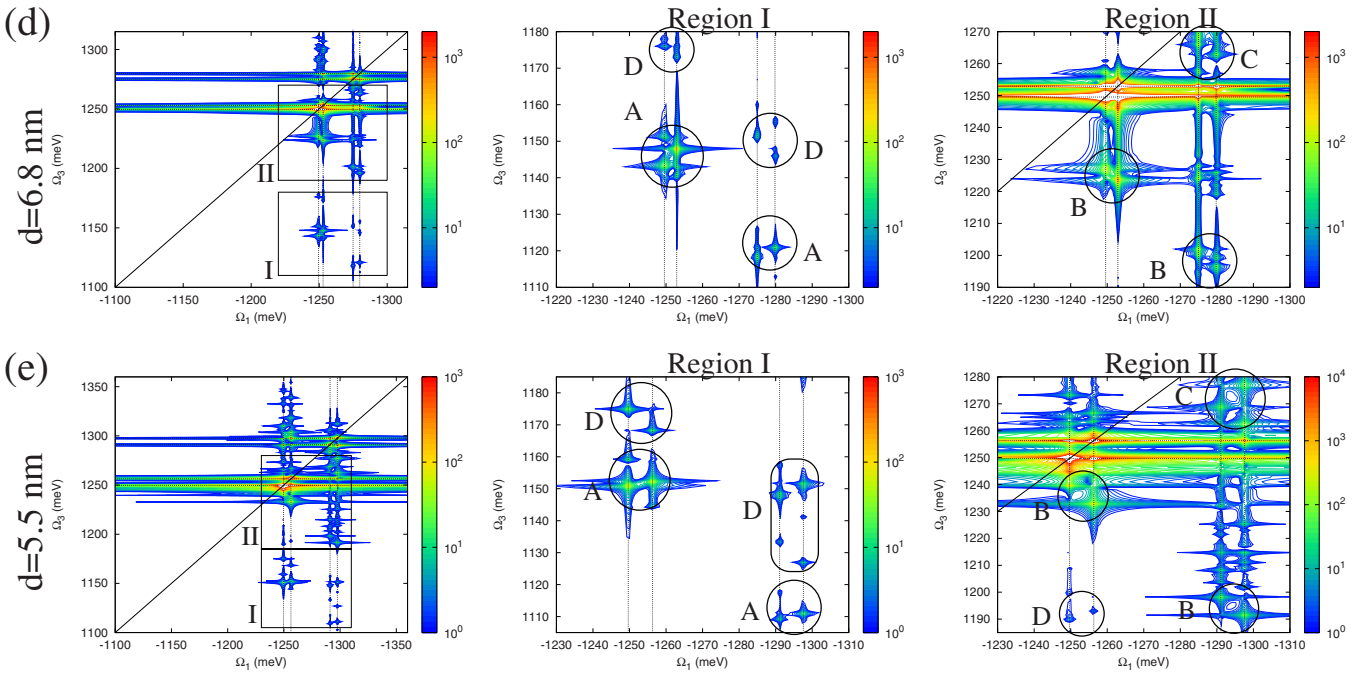

FIG. 9. (Color online) Absolute value of the $\mathbf{k}_{\mathrm{I}}$ signal for *xxxx* polarization without dipole-dipole interactions.

$\hat{B}_m$, $i\frac{d}{dt}\langle\hat{B}_m\rangle=\langle[\hat{B}_m,H]\rangle$, obtained by Eqs. (A1) and (A7),

$$i\frac{d}{dt}\langle\hat{B}_m\rangle=\sum_n h_{mn}\langle\hat{B}_n\rangle+\sum_{nkl}V_{mn,kl}\langle\hat{B}_n^\dagger\hat{B}_k\hat{B}_l\rangle-\boldsymbol{\mu}_m^*\cdot\mathbf{E}(t)$$
$$+2\sum_{nkl}\boldsymbol{\mu}_n^*\cdot\mathbf{E}(t)P_{mk,nl}\langle\hat{B}_k^\dagger\hat{B}_l\rangle. \quad \text{(B1)}$$

The last term in the right-hand side is known in the context of the simpler semiconductor Bloch equations as phase-space filling.[30] The second term describes exciton-exciton interactions where V is given by

$$V_{mn,kl}=U_{mn,kl}+U_{mn,kl}-2\sum_p P_{mn,pk}h_{pl}-2\sum_{pq}P_{mn,pq}U_{pq,kl}$$
$$=\bar{U}_{mn,kl}+\bar{U}_{mn,kl}-2\sum_p P_{mn,pk}h_{pl}-2\sum_{pq}P_{mn,pq}\bar{U}_{pq,kl}. \quad \text{(B2)}$$

Note that it is independent of the matrix F, Eq. (A5).

Similarly, for the two-particle variable, $\langle\hat{B}_m\hat{B}_n\rangle$, to second order in the optical field,

$$i\frac{d}{dt}\langle\hat{B}_m\hat{B}_n\rangle=\sum_{kl}h^{(2)}_{mn,kl}\langle\hat{B}_k\hat{B}_l\rangle-[\boldsymbol{\mu}_m^*\cdot\mathbf{E}(t)\langle\hat{B}_n\rangle+\langle\hat{B}_m\rangle\boldsymbol{\mu}_n^*\cdot\mathbf{E}(t)]$$
$$+2\sum_{kl}\boldsymbol{\mu}_l^*\cdot\mathbf{E}(t)P_{mn,kl}\langle\hat{B}_k\rangle, \quad \text{(B3)}$$

where

$$h^{(2)}_{mn,kl}=\delta_{mk}h_{nl}+\delta_{nl}h_{mk}+V_{mn,kl}. \quad \text{(B4)}$$

The diagonal elements of $h^{(2)}$ represent two electron-hole pair energies, while $V_{mn,mn}$ describes the biexciton binding energy. To see that, we use the definition of the electron-hole pair operators [Eq. (10)] the anticommutation relations (3) and (4), and Eqs. (A2)–(A6) to recast the V matrix in the form

$$V_{mn,kl}=V^{ee}_{m_1n_1}\delta_{m_1l_1}\delta_{n_1k_1}\delta_{m_2k_2}\delta_{n_2l_2}+V^{hh}_{m_2n_2}\delta_{m_1k_1}\delta_{n_1l_1}\delta_{m_2l_2}\delta_{n_2k_2}$$
$$+\frac{1}{2}(V^F_{m_1n_2k_1l_2}\delta_{n_1l_1}\delta_{m_2k_2}+V^F_{m_1n_2l_1k_2}\delta_{n_1k_1}\delta_{m_2l_2})$$
$$+\frac{1}{2}(V^F_{n_1m_2l_1k_2}\delta_{m_1k_1}\delta_{n_2l_2}+V^F_{n_1m_2k_1l_2}\delta_{m_1l_1}\delta_{n_2k_2})$$
$$-\frac{1}{2}(V^{eh}_{m_1n_2}+V^{eh}_{n_1m_2})\delta_{m_1k_1}\delta_{n_1l_1}\delta_{m_2k_2}\delta_{n_2l_2}-\frac{1}{2}(V^{eh}_{m_1n_2}$$
$$+V^{eh}_{n_1m_2})\delta_{m_1l_1}\delta_{n_1k_1}\delta_{m_2l_2}\delta_{n_2k_2}. \quad \text{(B5)}$$

This expression, which is the same as Eq. (20) in Ref. 25, clearly shows that V describes Coulomb interactions between the particles that constitute the two pairs.

Neglecting incoherent exciton transport, we can make the factorization,[36]

$$\langle\hat{B}_k^\dagger\hat{B}_l\rangle=\langle\hat{B}_k^\dagger\rangle\langle\hat{B}_l\rangle \quad \text{and} \quad \langle\hat{B}_n^\dagger\hat{B}_k\hat{B}_l\rangle=\langle\hat{B}_n^\dagger\rangle\langle\hat{B}_k\hat{B}_l\rangle. \quad \text{(B6)}$$

By expanding the equations of motion in orders of the optical field $E(t)$, and defining $B_m=\langle\hat{B}_m\rangle$, $Y_{mn}=\langle\hat{B}_m\hat{B}_n\rangle$, we finally obtain the nonlinear exciton equations,[27,28]

$$i\frac{d}{dt}B^{(1)}_m=\sum_n h_{mn}B^{(1)}_n-\boldsymbol{\mu}_m^*\cdot\mathbf{E}(t), \quad \text{(B7)}$$

$$i\frac{d}{dt}Y^{(2)}_{mn} = \sum_n h^{(2)}_{mn,kl}Y^{(2)}_{kl} - [\boldsymbol{\mu}^*_m \cdot \mathbf{E}(t)B^{(1)}_n + B^{(1)}_m \boldsymbol{\mu}^*_n \cdot \mathbf{E}(t)] + 2\sum_{kl} \boldsymbol{\mu}^*_l \cdot \mathbf{E}(t)P_{mn,kl}B^{(1)}_k, \tag{B8}$$

$$i\frac{d}{dt}B^{(3)}_m = \sum_n h_{mn}B^{(3)}_n + \sum_{nkl} V_{mn,kl}B^{(1)*}_n Y^{(2)}_{kl} + 2\sum_{nkl} \boldsymbol{\mu}^*_n \cdot \mathbf{E}(t)P_{mk,nl}B^{(1)*}_k B^{(1)}_l. \tag{B9}$$

APPENDIX C: THE 2D SIGNALS

The NEE equations may be solved using the single-exciton Green's functions and the exciton scattering matrix.[27] The polarization is then expressed in terms of the response function,

$$V^{\nu_4}(t) = \int dt_1 dt_2 dt_3 S^{\nu_4\nu_3\nu_2\nu_1}(t_3,t_2,t_1) \times E^{\nu_3}(t-t_3)E^{\nu_2}(t-t_3-t_2)E^{\nu_1}(t-t_3-t_2-t_1). \tag{C1}$$

The response function in the $\mathbf{k}_{\mathrm{I}}=-\mathbf{k}_1+\mathbf{k}_2+\mathbf{k}_3$ direction is given by[17]

$$S^{\nu_4\nu_3\nu_2\nu_1}_{\mathrm{I}}(\Omega_3,t_2,\Omega_1) = 2i\sum_{e_1,e_2,e_3,e_4} \mu^{\nu_1}_{e_1}\mu^{\nu_2*}_{e_2}\mu^{\nu_3*}_{e_3}\mu^{\nu_4}_{e_4} \times I^*_{e_1}(t_2)I_{e_2}(t_2)I^*_{e_1}(-\Omega_1)I_{e_4}(\Omega_3) \times \Gamma_{e_4e_1e_2e_3}(\Omega_3+E_{e_1}+i\gamma_{e_1}) \times \mathcal{G}_{0e_3e_2}(\Omega_3+E_{e_1}+i\gamma_{e_1}), \tag{C2}$$

where $\nu_1,\ldots,\nu_4$ are the polarizations of the optical pulses, $e_1,\ldots,e_4$ label eigenstates of the single-exciton block of the Hamiltonian with energies E_e and dephasing rates γ_e,

$$I_e(t) \equiv \langle e|\hat{G}(t)|e\rangle = -i\theta(t)e^{-iE_et-\gamma_et}, \tag{C3}$$

$$I_e(\omega) \equiv \langle e|\hat{G}(\omega)|e\rangle = (\omega - E_e + i\gamma_e)^{-1}, \tag{C4}$$

and $G(t)$ is the single-exciton Green's function. The Fourier transform is defined as

$$G(\omega) = \int dt\, \exp(i\omega t)G(t), \tag{C5}$$

$$G(t) = \int \frac{d\omega}{2\pi}\exp(-i\omega t)G(\omega). \tag{C6}$$

Finally,

$$\mathcal{G}_{0e_2e_1}(\omega) \equiv \langle e_1e_2|\hat{\mathcal{G}}_0(\omega)|e_1e_2\rangle = \frac{1}{\omega - E_{e_2} - E_{e_1} + i(\gamma_{e_2}+\gamma_{e_1})} \tag{C7}$$

is the Green's function representing noninteracting two excitons, and the scattering matrix is given by

$$\Gamma(\omega) = [\mathbb{I} - V\mathcal{G}_0(\omega)]^{-1}V\mathcal{G}_0(\omega)(\mathbb{I}-P)\mathcal{G}_0^{-1}(\omega) - P\mathcal{G}_0^{-1}(\omega), \tag{C8}$$

where V is given in Eq. (B5), and $\mathbb{I}$ is the tetradic identity matrix in the two-exciton space.

Similarly, the response in the $\mathbf{k}_{\mathrm{III}}$ direction is given by[17]

$$S^{\nu_4\nu_3\nu_2\nu_1}_{\mathrm{III}}(\Omega_3,\Omega_2,t_1) = 2\sum_{e_1,e_2,e_3,e_4} \mu^{\nu_1*}_{e_1}\mu^{\nu_2*}_{e_2}\mu^{\nu_3}_{e_3}\mu^{\nu_4}_{e_4} \times I^*_{e_1}(t_1)I_{e_4}(\Omega_3)I^*_{e_3}(\Omega_2-\Omega_3) \times [\Gamma_{e_4e_3e_2e_1}(\Omega_3+E_{e_3}+i\gamma_{e_3})\mathcal{G}_{0e_2e_1}(\Omega_3 + E_{e_3}+i\gamma_{e_3}) - \Gamma_{e_4e_3e_2e_1}(\Omega_2)\mathcal{G}_{0e_2e_1}(\Omega_2)]. \tag{C9}$$

[1] A. D. Yoffe, Adv. Phys. **50**, 1 (2001).
[2] G. D. Scholes and G. Rumbles, Nature Mater. **5**, 683 (2006).
[3] V. I. Klimov, Annu. Rev. Phys. Chem. **58**, 635 (2007).
[4] X. Peng, L. Manna, W. Yang, J. Wickham, E. Scher, A. Kadavanich, and A. P. Alivisatos, Nature (London) **404**, 59 (1999).
[5] B. Fisher, J.-M. Caruge, Y.-T. Chan, J. Halpert, and M. G. Bawendi, Chem. Phys. **318**, 71 (2005).
[6] X. Xu, B. Sun, P. R. Berman, D. G. Steel, A. S. Bracker, D. Gammon, and L. J. Sham, Science **317**, 929 (2007).
[7] M. Bruchez, Jr., M. Moronne, P. Gin, S. Weiss, and A. P. Alivisatos, Science **281**, 2013 (1998).
[8] V. I. Klimov, A. A. Mikhailovsky, S. Xu, A. Malko, J. A. Hollingsworth, C. A. Leatherdale, H.-J. Eisler, and M. G. Bawendi, Science **290**, 314 (2000).
[9] J.-W. Luo, A. Franceschetti, and A. Zunger, Nano Lett. **8**, 3174 (2008).
[10] A. Imamoglu, D. D. Awschalom, G. Burkard, D. P. DiVincenzo, D. Loss, M. Sherwin, and A. Small, Phys. Rev. Lett. **83**, 4204 (1999).
[11] P. Zanardi and F. Rossi, Phys. Rev. Lett. **81**, 4752 (1998).
[12] O. Gywat, G. Burkard, and D. Loss, Phys. Rev. B **65**, 205329 (2002).
[13] G. Allan and C. Delerue, Phys. Rev. B **75**, 195311 (2007).
[14] A. Sitek and P. Machnikowski, Phys. Rev. B **75**, 035328 (2007).
[15] M. Bayer, P. Hawrylak, K. Hinzer, S. Fafard, M. Korkusinski, Z. R. Wasilewski, O. Stern, and A. Forchel, Science **291**, 451 (2001).
[16] G. Bester, J. Shumway, and A. Zunger, Phys. Rev. Lett. **93**, 047401 (2004).
[17] R. Oszwaldowski, D. Abramavicius, and S. Mukamel, J. Phys.: Condens. Matter **20**, 045206 (2008).
[18] S. Mukamel, Ann. Rev. Phys. Chem. **51**, 691 (2000).
[19] G. S. Engel, T. R. Calhoun, E. L. Read, T.-K. Ahn, T. Mancal, C. Yuan-Chung, R. Blankenship, and G. R. Fleming, Nature (Lon-

don) **446**, 782 (2007).
[20] L. Yang, I. V. Schweigert, S. T. Cundiff, and S. Mukamel, Phys. Rev. B **75**, 125302 (2007).
[21] W. Langbein and B. Patton, J. Phys.: Condens. Matter **19**, 295203 (2007).
[22] X. Li, T. Zhang, S. Mukamel, R. Mirin, and S. T. Cundiff, Solid State Commun. **149**, 361 (2009).
[23] T. Meier, P. Thomas, and S. W. Koch, *Coherent Semiconductor Optics: From Basic Concepts to Nanostructure Applications* (Springer, New York, 2006).
[24] G. Bester, A. Zunger, and J. Shumway, Phys. Rev. B **71**, 075325 (2005).
[25] V. Chernyak and S. Mukamel, J. Opt. Soc. Am. B **13**, 1302 (1996).
[26] S. Mukamel, *Principles of Nonlinear Optical Spectroscopy* (Oxford University Press, New York, 1995).
[27] S. Mukamel, R. Oszwaldowski, and D. Abramavicius, Phys. Rev. B **75**, 245305 (2007).
[28] V. Chernyak, W. M. Zhang, and S. Mukamel, J. Chem. Phys. **109**, 9587 (1998).
[29] M. Combescot and O. Betbeder-Matibet, Phys. Rev. B **78**, 125206 (2008).
[30] H. Haug and S. W. Koch, *Quantum Theory of the Optical and Electronic Properties of Semiconductors*, 4th ed. (World Scientific, Singapore, 2004).
[31] B. W. Lovett, J. H. Reina, A. Nazir, and G. A. D. Briggs, Phys. Rev. B **68**, 205319 (2003).
[32] R. Baer and E. Rabani, J. Chem. Phys. **128**, 184710 (2008).
[33] *Optical Orientation*, edited by F. Meier and B. P. Zakharchenya, Modern Problems in Condensed Matter Sciences Vol. 8 (North-Holland, Amsterdam, 1984).
[34] S. C. K. L. Silverman, R. P. Mirin, and A. G. Norman, Appl. Phys. Lett. **82**, 4552 (2003).
[35] D. Abramavicius, B. Palmieri, D. V. Voronine, F. Šanda, and S. Mukamel, Chem. Rev. (Washington, D.C.) (to be published).
[36] S. Mukamel, in *Molecular Nonlinear Optics*, edited by J. Zyss (Academic Press, New York, 1994), Chap. 1, pp. 1–46.